Available online at www.sciencedirect.com

jmr&t Journal of Materials Research and Technology

journal homepage: www.elsevier.com/locate/jmrt

Original Article

Numerical and experimental study of porous NiTi anisotropy under compression

Ekaterina S. Marchenko [a], *Alexander A. Kozulin* [a], *Yuri F. Yasenchuk* [a], *Anna V. Vetrova* [a], *Alex A. Volinsky* [a,b,*], *Yi Zhang* [c]

[a] *Laboratory of Superelastic Biointerfaces, National Research Tomsk State University, Tomsk, 634050, Russia*
[b] *Department of Mechanical Engineering, University of South Florida, Tampa, 4202 E. Fowler Ave. ENG 030, FL, 33620, USA*
[c] *School of Materials Science and Engineering, Henan University of Science and Technology, Luoyang, 471023, PR China*

ARTICLE INFO

Article history:
Received 20 October 2022
Accepted 27 December 2022
Available online 31 December 2022

Keywords:
Porous NiTi
Compression
Modeling
Anisotropy
Orthotropy
Computed tomography

ABSTRACT

Porous NiTi samples were obtained by self-propagating high-temperature synthesis (SHS) and cut to specific dimensions by electrical discharge machining. Quasi-static compression of the porous SHS-NiTi alloy demonstrated that the deformation was elastic-plastic. Three characteristic types of fracture surfaces of bridges can be distinguished. 1) Ductile fracture of the austenite phase in the form of a cup and cone relief. 2) Brittle fracture with the formation of cleavage steps. 3) Large areas of plastic shear, where cup and cone, and cleavage facets are nucleated. An algorithm for obtaining a porous framework model suitable for finite element method calculations has been developed. The effective moduli of elasticity and shear for the porous volume of the material were determined. It is shown that the studied porous volume has orthotropic elastic properties due to the geometry of the porous framework.

1. Introduction

Porous materials with inelastic mechanical behavior are quite common among natural and artificial materials and in the human body. Most of these materials have a complex porous structure. The manufacturing of implant materials results in different degrees of porosity due to variations in technological processes. Porous nitinol (NiTi) alloys occupy a special place among implant materials [1–4]. In many cases, porous implants and bone tissues are hierarchically organized multiscale systems. The structure of a porous framework with open porosity has anisotropy, which is divided into anisotropy of mechanical properties, structural anisotropy [5], and geometric anisotropy [6]. Such systems accumulate multiscale damage under external loads and form new structures, making their mechanical response even more complicated. The problem of porous materials' deformation occurring under special conditions has not been sufficiently studied. The use of global stresses and strains cannot be utilized inside a porous

* Corresponding author.
E-mail address: volinsky@usf.edu (A.A. Volinsky).
https://doi.org/10.1016/j.jmrt.2022.12.168

body, so local stresses and strains need to be obtained using finite element analysis. One of the fundamental problems in modeling these systems is the construction of constitutive equations that describe all aspects of their mechanical behavior, including the deformation response and fracture. Such constitutive equations should take into account both the characteristic features of local damage accumulation and the evolution of the pore space under various loading conditions [7]. Extensive literature is devoted to modeling the deformation of porous materials [8–14]. These studies cover several areas: a) porous volume modeling, b) determination of constants for equations describing a porous medium, and c) direct numerical simulation of the deformation and fracture processes of porous materials.

An effective approach to the study of such systems is the evolutionary methodology developed by the authors [15–17]. From a mathematical point of view, the complete system of differential equations of continuum mechanics, together with the constitutive relations, describing the non-stationary behavior of solid deformable bodies, is a system of nonlinear dynamic equations. From a physical point of view, the loaded material is considered a nonlinear dynamic multiscale system. Nonlinear positive and negative feedbacks are explicitly set in the system, which regulate the interaction between the stress-strain state of the material and the response of the material to loading in the form of damage accumulation at different scales and degradation of strength properties. Such an approach makes it possible to effectively describe the evolution of the properties of porous materials at different levels, including localized accumulation of damage and inelastic deformations, strength degradation, and the formation of cracks of various scales, including the main cracks leading to macroscopic fracture. Therefore, the purpose of this work is to study the anisotropy of properties due to the geometric aspects of the porous framework, which must be explicitly taken into account in geometric models when predicting the behavior of medical devices made of porous nitinol used as implants.

2. Materials and methods

2.1. Uniaxial compression of porous nitinol

A porous cylindrical blank with a 20 mm diameter, and 120 mm height was made from nitinol by the self-propagating high-temperature synthesis (SHS, continuous layer-by-layer combustion) in a protective argon gas atmosphere from a 50% Ni and 50% Ti powder mixture. PTOM-2 titanium powder up to 50 μm reduced with calcium hydride and PNKOT-4 nickel powder up to 50 μm with carbonyl fraction were used. The powder mixture was placed in a cylindrical quartz tube and heated in a compact electric resistance furnace. The synthesis starting temperature was selected experimentally. A porous ingot was obtained at 460±10 °C. The sample had a unimodal pore size distribution close to normal. Prismatic 6×3×3 mm^3 samples were cut from a cylindrical billet shown in Fig. 1. Stress-strain curves for evaluating the mechanical properties of porous NiTi were obtained by uniaxial compression using INSTRON 3369 universal tensile testing machine with 6×3×3 mm^3 prismatic samples of porous nitinol until failure at a 0.2 mm/min loading rate. The microstructure and fracture surfaces were studied using a Tescan Vega 3 SBH scanning electron microscope equipped with an Oxford Instruments Aztec Live Lite Xplore 30 energy dispersive microanalysis system operated at an accelerating voltage of 20 kV in 9×10^{-3} Pa vacuum.

2.2. Porous nitinol model

In order to carry out numerical calculations to determine the stress-strain behavior, it is necessary to prepare a geometric model suitable for use in the finite element method. The authors developed an algorithm for obtaining a solid-state CAD model suitable for finite element calculations. To do this, the following steps were taken.

Fig. 1 – Porous nitinol ingots obtained by the SHS method.

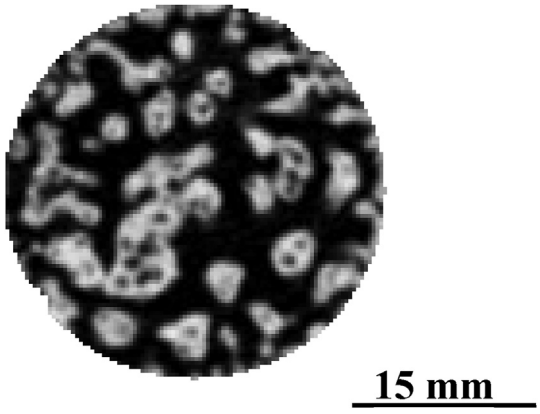

Fig. 2 – 2D X-ray image of the nitinol sample section with large pores obtained by X-ray tomography.

1. The results of 3D computed X-ray tomography were obtained as an array of files with layer-by-layer transverse and longitudinal images of a porous nitinol sample with sufficient resolution and details. The 3D tomography data were obtained in the neutron research complex based on the IR-8 reactor of the National Research Center "Kurchatov Institute" with the following parameters. Monochromatic neutron flux energy of 46 keV, 75×75 mm^2 dimensions of the incident neutron beam cross-section, 2.4 Å wavelength, 3.6×10^6 neutrons/cm^2/s neutron flux density on the sample, 200 μm spatial resolution, and 0.8 s exposure. Fig. 2 shows an image of a sample cross-section.
2. All images were adjusted for the degree of structural elements susceptibility using special software with eliminated X-ray tomography artifacts. The sequentially obtained layer-by-layer images were overlayed and the reconstruction of the porous volume of the alloy was saved in the STL format using the InVesalius 3.2 software (Fig. 3).
3. The resulting STL model was subjected to additional processing in the SpaceClaim solid-state modeling software package and a 3D volumetric reconstruction of the model was obtained in the form of a CAD file for transfer to any engineering analysis software package using the finite element method. The STL file obtained at the second stage contained information about the 3D model in the form of a list of triangular faces that bound a certain volume. This format was originally invented for additive technologies and is still successfully used in 3D printing. However, this format is not suitable for use in calculations. Fig. 4 shows the final view of the solid model prepared for numerical simulations.

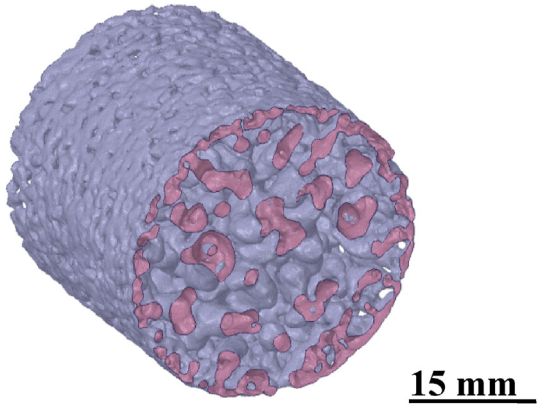

Fig. 3 – The STL model of a porous body obtained by processing the X-ray tomography images.

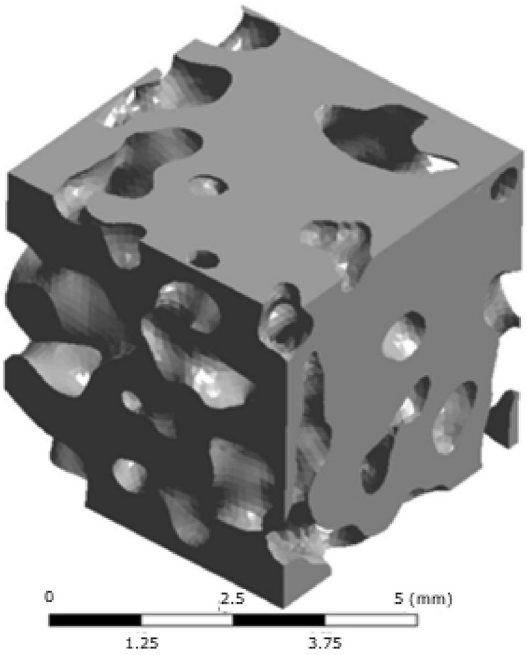

Fig. 4 – CAD model of the porous representative volume used in the calculations.

2.3. *Mathematical statement of the problem*

The stress-strain state of a porous nitinol representative volume element under uniaxial and shear loading was solved. Numerical solutions were used to determine the effective elastic moduli and Poisson's ratios in three perpendicular directions. The mathematical model for solving the problem was represented by a system of continuum mechanics differential equations in a general form. The system of equations consisted of equilibrium equations, the Cauchy geometric relations, and constitutive relations in the form of Hooke's law. The system of equations was solved numerically using the finite element method and the Lagrange approach in a Cartesian rectangular coordinate system (x_1, x_2, x_3)

$$\sigma_{ij,j} = 0, \tag{1}$$

$$\varepsilon_{kl} = \frac{1}{2}(u_{l,k} + u_{k,l}), \tag{2}$$

$$\sigma_{ij} = E_{ijkl}\varepsilon_{kl}, \tag{3}$$

here, $\sigma_{ij} = \sigma_{ji}$ (i, j, k, l = 1, 2, 3) are symmetric stress tensor components, $\varepsilon_{ij} = \varepsilon_{ji}$ are strain tensor components, ε_{ij}^{el} are elastic strain values, u_i and u_j are displacement vector

components, and E_{ijkl} are components of the fourth order stiffness tensor. The comma before the index means differentiation with respect to the spatial coordinate. When performing these calculations, it was assumed that the material of the porous samples was isotropic. The following initial nitinol properties were used: E = 74 GPa Young's modulus, $\nu = 0.3$ Poisson's ratio, $\mu = 28$ GPa shear modulus, and 6650 kg/m^3 density. Fig. 5 shows an example of a finite element model of representative volume used in the calculations prepared based on the CAD model in Fig. 4. For the convenience of representing the boundary conditions, the figure shows a Cartesian rectangular coordinate system x_1, x_2, and x_3. Uniaxial compression was along the x_2 axis.

The effective elastic moduli and Poisson's ratios in three perpendicular directions for a porous sample were determined based on the elastic response of the system obtained numerically for the 6 loading conditions (3 normal and 3 shear). The following boundary conditions were used for the calculations. Boundary conditions on the faces normal to the x_1-axis (4), x_2-axis (5), and x_3-axis (6) for uniaxial compression in three directions are

$$u_{x1}(L_{x1}, x_2, x_3) = -\varepsilon_{x1} L_{x1}, u_{x1,x2,x3}(0, x_2, x_3) = 0 \quad (4)$$

$$u_{x2}(x_1, L_{x2}, x_3) = -\varepsilon_{x2} L_{x2}, u_{x1,x2,x3}(x_1, 0, x_3) = 0 \quad (5)$$

$$u_{x1}(x_1, x_2, L_{x3}) = -\varepsilon_{x3} L_{x3}, u_{x1,x2,x3}(x_1, x_2, 0) = 0 \quad (6)$$

here, L_{x1}, L_{x2}, L_{x3} are distances between faces of a representative volume normal to the x_1, x_2, and x_3-axis, respectively. ε_{x1}, $\varepsilon_{x2}, \varepsilon_{x3}$ are predefined values of small normal strains with respect to the x_1, x_2, and x_3-axis.

The boundary conditions for the shear x_1x_2 case are set as follows (7–9).

- on faces normal to the x_1-axis

$$u_{x2}(L_{x1}, x_2, x_3) = \gamma L_{x1}, \quad (7)$$

$$u_{x2,x3}(0, x_2, x_3) = 0,$$

$$u_{x3}(L_{x1}, x_2, x_3) = 0.$$

- on faces normal to the x_2-axis

$$u_{x1,x3}(x_1, 0, x_3) = 0,$$

$$u_{x1,x3}(x_1, L_{x2}, x_3) = 0, \quad (8)$$

- on faces normal to the x_3-axis

$$u_{x3}(x_1, x_2, 0) = 0,$$

$$u_{x3}(x_1, x_2, L_{x3}) = 0. \quad (9)$$

here, γ are predefined values of small shear strains. The boundary conditions for shear x_1x_3 case from (7–9) can be obtained by switching the roles of x_2 and x_3. The boundary conditions for shear x_2x_3 case can be obtained by switching the roles of x_1 and x_2, starting from the shear x_1x_3 case.

The system of equations of the linear theory of elasticity in the (1–3) form with the corresponding boundary conditions (4–9) is a tool for determining the stress-strain state of the material and the elastic response of the investigated representative volume element. To describe the mechanical behavior of the investigated representative volume element of porous nitinol in the continuum approximation, it is necessary to determine the values of the stiffness tensor and compliance tensor components of an anisotropic material. To achieve this, equation (3) can be reduced to the following constitutive relationship:

$$\varepsilon_{ij} = S_{ijkl}\sigma_{kl} \quad (10)$$

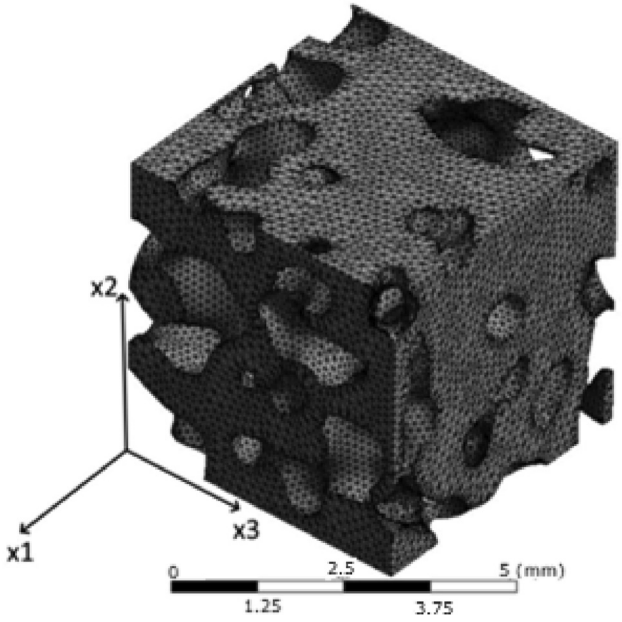

Fig. 5 – Finite element model of the porous nitinol representative volume element used in the calculations.

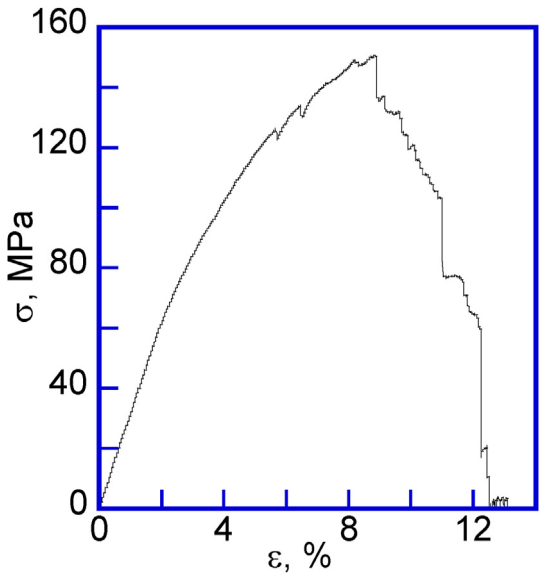

Fig. 6 – Typical experimental engineering stress-strain curve obtained under uniaxial quasistatic compression of porous SHS-NiTi with 6×3×3 mm^3 dimensions.

Table 1 – Mechanical properties of porous nitinol under uniaxial compression.

Specimen dimensions, length × width × thickness, mm^3	Elastic limit, MPa	Compressive strength, MPa	Elastic modulus, GPa	Elastic strain, %	Plastic strain, %	Total strain at failure, %
6×3×3	61.8 ± 5	153 ± 16	3.2 ± 0.1	1.9 ± 0.1	7.2 ± 0.6	9.1 ± 0.8

here, S_{ijkl} are components of the fourth-order compliance tensor. The components E_{ijkl} in equation (3) have symmetry properties [2,5].

$$E_{ijkl} = E_{jikl} = E_{klij} \tag{11}$$

The constants S_{ijkl} also satisfy the symmetry conditions (11) and are related to E_{ijkl}

$$E_{ijkl}S_{klrs} = \delta_{ijrs} \equiv \left(\delta_{ir}\delta_{js} + \delta_{is}\delta_{jr}\right)/2, S_{klrs}E_{ijkl} = \delta_{ijrs} \tag{12}$$

here, $\delta_{ij} = 1$ at $i = j$, and $\delta_{ij} = 0$ at $i \neq j$. The unit tensor δ_{ijrs} is in the symmetric tensors space of the form (11). Let n_i and m_i ($i = 1, 2, 3$) be two orthogonal unit directions. The Young's moduli E_n in the n_i direction from S_{ijkl} is defined as

$$\frac{1}{E_n} = n_i n_j S_{ijkl} n_k n_l \tag{13}$$

Poisson's ratio ν_{mn} in the direction m_i under tension applied in the direction n_i is equal to

$$\frac{\nu_{mn}}{E_n} = -m_i m_j S_{ijkl} n_k n_l \tag{14}$$

On the left side of equation (14), summation over n is not carried out. The shear modulus μ_{nm} between the sites with normal n_i and m_i is equal to

$$\frac{1}{4\mu_{nm}} = n_i m_j S_{ijkl} n_k m_l \tag{15}$$

The bulk modulus is presented in the form of $1/K = S_{ijkl}$. Thus, knowing the stress-strain state in six loading conditions, after using the boundary conditions (4–9), one can determine 9 components (13), (14), and (15) of the compliance tensor, from which the effective elastic moduli (E_1, E_2, E_3, μ_{12}, μ_{23}, μ_{31}) and Poisson's ratios (ν_{12}, ν_{23}, ν_{31}) are found for an orthotropic medium describing the mechanical behavior of the studied porous representative volume element in the continuum approximation.

3. Results

3.1. *Quasistatic uniaxial compression of porous nitinol*

Fig. 6 shows a typical engineering stress-strain curve of the five tested 6×3×3 mm^3 porous NiTi samples. From the engineering stress-strain curves obtained by quasi-static uniaxial compression until the failure of the porous nitinol sample, the elastic limit and compressive strength were determined, listed in Table 1. The characteristic yield areas associated with the martensitic transformations caused by stress are not present in the stress-strain curve. The stress-strain curve has a characteristic form of elastic-plastic deformation with hardening. In the softening area, the steps during failure indicate the brittle fracture of the bridges of the porous frame.

Fig. 7 – Porous SHS-NiTi sample after compression failure.

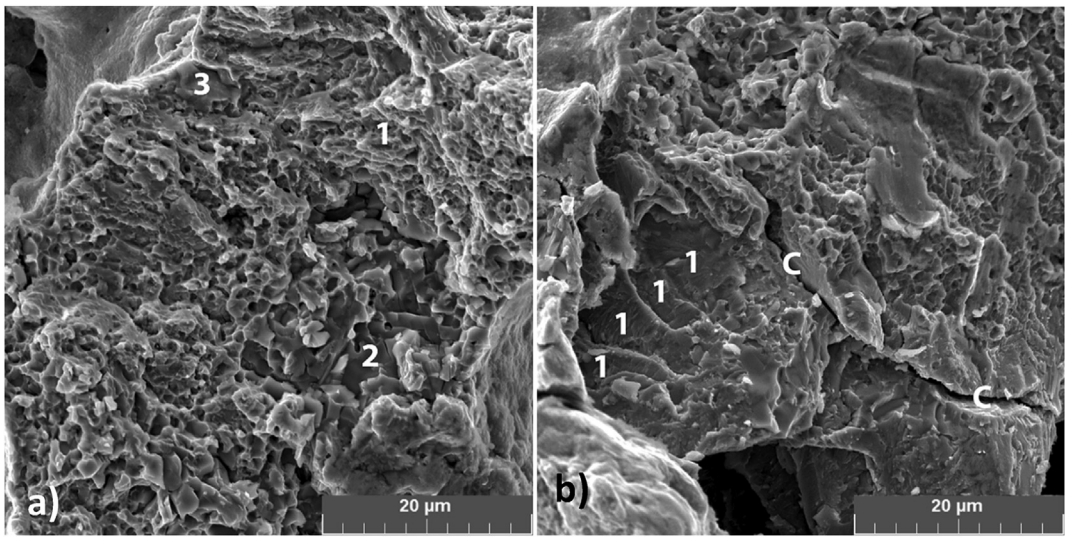

Fig. 8 – SEM images of the porous NiTi frame wall fracture surfaces: (a) mixed ductile and brittle fracture; (b) cup and cone reliefs. Here, 1 is the surface of ductile fracture, 2 is the peritectic intergranular phase with a sign of brittle fracture, 3 is non-metallic inclusions on the surface - sources of crack development, and C is a crack.

3.2. *Fracture surfaces of porous SHS-NiTi under quasistatic compression*

Fig. 7 shows a fractured porous SHS-NiTi sample, which is macroscopically fractured at a 45° angle to the compression direction under the action of tangential shear stresses. Thus, it can be argued that the stress localization during compression of a porous SHS-NiTi alloy occurs according to the classical mechanisms of the mechanics of materials. Fig. 8 is a scanning electron microscopy (SEM) image of the porous NiTi frame wall fracture surface. The nature of the porous frame wall fracture is a mixed, predominantly viscous failure. A large number of viscous shear steps combined with cup and cone relief of ductile fracture 1 were found on the fracture surfaces in Fig. 8a. There are areas of brittle fracture facets with cracks 2, and surface cracks 3 in Fig. 8a.

Brittle cleavage steps occur among the predominantly ductile fracture. Large brittle cleavage cracks C run normally to the main fracture surface in Fig. 9. There are areas of viscous shear 2 on the ductile fracture surface 1, which look like cup and cone reliefs in Fig. 8b.

In Fig. 10 areas with brittle fracture facets and a large number of cracks propagating perpendicular to the main fracture surface belong to the brittle Ti_2Ni phase distributed along the boundaries of austenite grains. Large surfaces of shear deformation of the austenite phase have a residual pit relief in Fig. 10. There is a section of the brittle phase stepped cleavage in the center of the ductile fracture surface of the austenitic phase with a cup and cone relief in Fig. 10.

Summarizing the quasi-static compression results of the porous SHS-NiTi alloy, three characteristic types of the fracture surfaces of the bridges can be distinguished: 1) Ductile fracture of the austenite phase in the form of a cup and cone relief, 2) brittle fracture with the formation of cleavage steps, 3) large areas of plastic shear deformation, where cups, cones, and cleavage facets are nucleated. The fracture of the porous framework walls is mainly ductile, indicating the predominance of the austenite phase TiNi(B2) at the initial stage of porous NiTi alloy fracture.

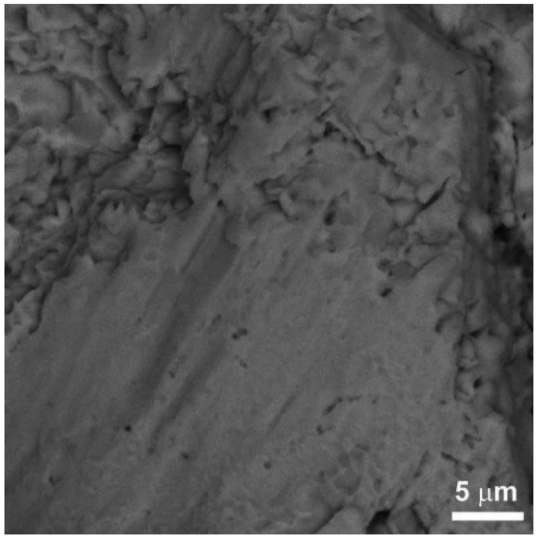

Fig. 9 – Fragment of the fracture surface with an area of viscous shear deformation.

3.3. *Volumetric model of porous NiTi*

Initial calculations were carried out to determine the anisotropy of the properties of a porous sample. For this, the effective moduli of elasticity and shear were determined for the porous volume of the material. A cube obtained based on the tomography results with $2.5\times2.5\times2.5$ mm^3 dimensions was considered. A mathematical model (1–3) with boundary conditions (4–9) makes it possible to evaluate the stress-strain state of the NiTi sample with explicit porosity. Carried computations already reveal the features of strain localization in

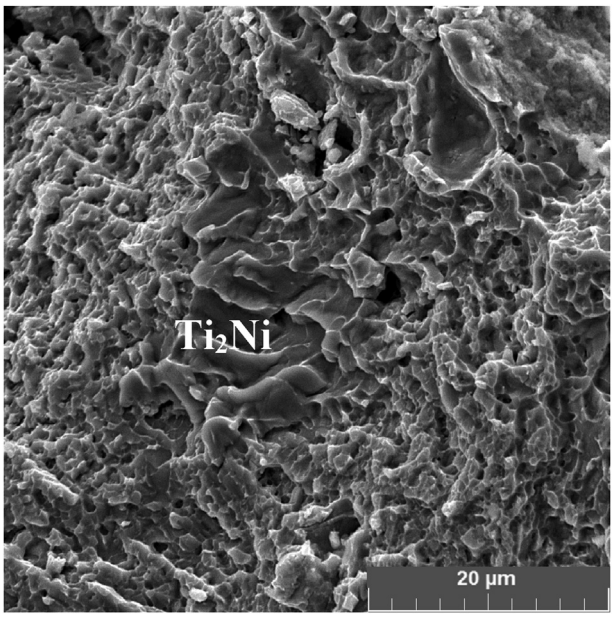

Fig. 10 – SEM image of the fracture surface fragment with a brittle stepped cleavage surrounded by a pitted relief of a ductile fracture.

the porous sample, characteristic of porous frame bridges. Figs. 11 and 12 show the areas of stress and strain concentration, where the conditional yield strength is reached. The values of equivalent strains correspond to the distribution of equivalent stresses in Fig. 12. Von Mises critical stress concentrations are located in areas with the maximum curvature of the frame surface and are shown in colors other than blue.

Computed stress and strain fields correspond to the localization of fracture sources and zones during compression until the porous NiTi alloy failure. The fracture surfaces of the porous alloy under tangential shear stresses lie at a 45° angle to the uniaxial compression direction. Thus, it can be argued that the porous NiTi alloys fracture according to the standard mechanisms described by the mechanics of solids under uniaxial compression. Computations of the porous sample compression in three perpendicular directions are sufficient to determine the effective elastic moduli. In this case, the properties are considered orthotropic, which is a special case of anisotropy.

Table 2 lists the calculation results, where the numbers 1, 2, and 3 correspond to the Cartesian coordinates x_1, x_2, and x_3.

Due to porosity, the calculated effective properties of the considered volume turned out to be less than the properties of the original non-porous material. When analyzing the results presented in Table 1, it was found that the value of Young's modulus varies depending on the direction of the coordinate axes in Fig. 13. The maximum value is along the x_2 axis and is equal to 3.24 GPa, and the minimum 2.98 GPa value is along the x_1 axis. Shear moduli and Poisson's ratio change within the 2% margin of error. The effective value of the considered porous cube density is 3551 kg/m^3, which is 66% less than the original non-porous material. It can be concluded from the presented results that the studied porous volume has an orthotropy of elastic properties due to the geometry of the porous framework. The random arrangement of the porous frame fracture surfaces with respect to the compressive load axis is the reason for the different nature of the fracture. During the fracture of the porous framework by a uniaxial compressive load, areas of viscous fracture and plastic shear of austenite TiNi(B2) were found. This is due to the fact that

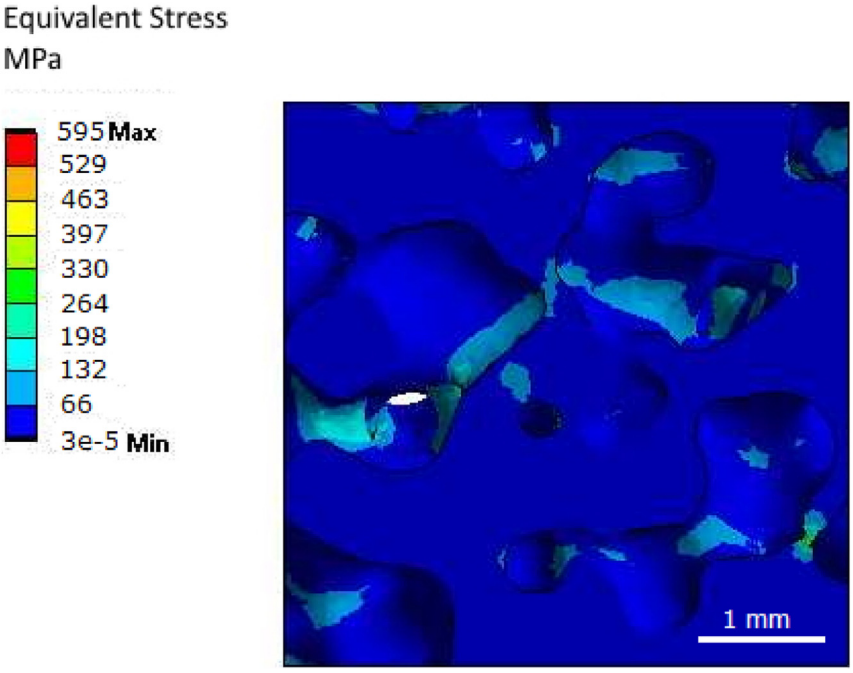

Fig. 11 – Distribution of equivalent stresses in the volume of the model under compression along the x_2 axis (view of one of the studied volume surfaces).

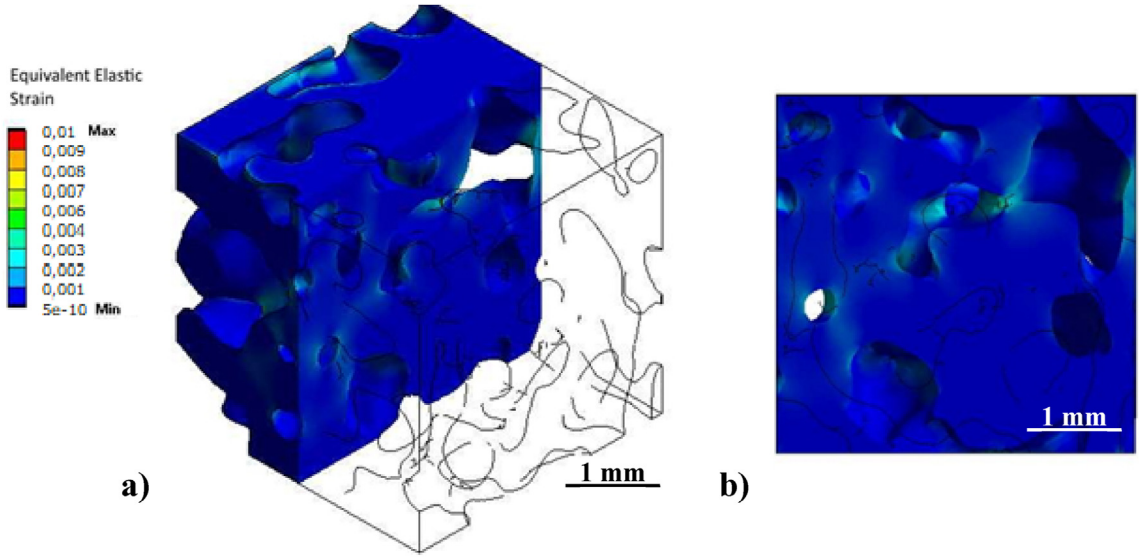

Fig. 12 – Distribution of equivalent strains in the volume of the model during compression along the x_2 axis: (a) isometric view of the model with a cross-section; (b) view of the $x_1x_2|_{x3=2.5\ mm}$ cross-section.

Table 2 – Calculation results of the effective moduli of elasticity, shear modulus and Poisson's ratios for the volume of the porous material.

Engineering constants	Value
E_1, GPa	2.98
E_2, GPa	3.24
E_3, GPa	3.01
μ_{12}, GPa	1.21
μ_{23}, GPa	1.31
μ_{31}, GPa	1.22
ν_{12}	0.231
ν_{13}	0.2375
ν_{23}	0.2332
Density ρ, kg/m^3	3551

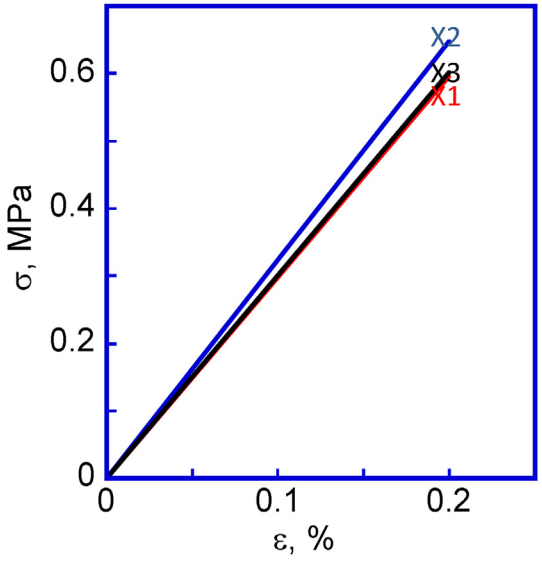

Fig. 13 – Calculated engineering elastic stress-strain curves of porous NiTi in three perpendicular directions.

areas of compression, shear, bending, and tension simultaneously appeared in the porous framework. In addition, areas of brittle cleavage of the brittle Ti_2Ni phases, non-metallic inclusions, and quasi-brittle cleavage of martensite TiNi(B19′) were found. The numerical model made it possible to determine the stress concentrators and areas of localized deformation at the elastic deformation stage (0.2%), long before the occurrence of plastic shear. These are areas of the greatest curvature of the porous framework walls around small pores. Plastic shear processes originated in areas of localized compression and shear. Bending areas appeared with the development of the deformation process. The processes of viscous separation with a pitted relief arose in the fracture areas, where the strain rate significantly exceeded the shear and bending rates and was close to the impact fracture rates. Porosity was explicitly taken into account in numerical simulations, since the finite element model of the porous framework was created from 3D reconstruction of the actual SHS-NiTi alloy porous framework. In a numerical experiment, the created porous frame model was elastically compressed to 0.2%. A porous NiTi alloy sample used for the reconstruction was deformed in compression to plastic failure at 9%. The results of physical and numerical experiments of the porous NiTi deformation process were compared and analyzed.

4. Conclusions

It has been established that the deformation is elastic-plastic during quasi-static compression of porous nitinol samples. The bridges of the porous framework fractured viscously but not simultaneously, which is characterized by a stepped softening stage. Three characteristic types of the fracture surfaces under quasi-static compression of the porous SHS-NiTi alloy are distinguished: 1) ductile fracture of the austenite phase in the form of a cup relief, 2) brittle fracture with the formation of cleavage steps, 3) large areas of plastic

shear deformation, where cups and cleavage facets are nucleated. It has been established that the predominant type of fracture in the walls of the porous framework is ductile, which indicates the predominance of the austenitic phase TiNi(B2) at the initial stage of porous nitinol fracture. An algorithm has been developed for obtaining a solid model of a porous framework suitable for use in finite element calculations.

The values of the calculated moduli of elasticity for the studied model of porous nitinol vary in the 2.98–3.24 GPa range and correspond to the experimental results of NiTi samples compression. When analyzing the theoretical and experimental results, it was found that the cause of fracture of a porous NiTi alloy under uniaxial compression is localized deformation in the areas of thinning of the frame bridges, where defects accumulate under the action of tangential shear stresses at the 45° angle to the uniaxial compression direction.

Declaration of competing interest

The authors declare that they have no known competing financial interests or personal relationships that could have appeared to influence the work reported in this paper.

Acknowledgments

This research was supported by the Mega grant from the Government of the Russian Federation No. 220 of April 9, 2010 (Agreement No. 075-15-2021-612 of June 4, 2021). Characterization was carried out using the equipment of Tomsk Regional Core Shared Research Facilities Center of National Research Tomsk State University (Grant of the Ministry of Science and Higher Education of the Russian Federation No. 075-15-2021-693, 13. RFC.21.0012).

REFERENCES

[1] Li BY, Rong L, Li Y, Gjunter VE. Synthesis of porous Ni-Ti shape-memory alloys by self-propagating high-temperature synthesis: reaction mechanism and anisotropy in pore structure. Acta Mater 2000;48:3895–904. https://doi.org/10.1016/S1359-6454(00)00184-1.

[2] McNaney J, Imbeni V, Jung Y, Papadopoulos P, Ritchie R. An experimental study of the superelastic effect in a shape-memory Nitinol alloy under biaxial loading. Mech Mater 2003;35:969–86. https://doi.org/10.1016/S0167-6636(02)00310-1.

[3] Marchenko ES, Klopotov AA, Ustinov AM, Abzaev Yu A, Vetrova AV, Garin AS, et al. Study of macroplastic flow in surface layers of porous titanium nickelide by digital image correlation. In: AIP conference proceedings, vol. 2509; 2022. p. 20129. https://doi.org/10.1063/5.0085185.

[4] Monogenov AN, Marchenko ES, Baigonakova GA, Yasenchuk YuF, Garin AS, Volinsky AA. Improved mechanical properties of porous nitinol by aluminum alloying. J Alloys Compd 2022;918:165617. https://doi.org/10.1016/j.jallcom.2022.165617. A.

[5] Kang J, Dong E, Li D, Dong S, Zhang C, Wang L. Anisotropy characteristics of microstructures for bone substitutes and porous implants with application of additive manufacturing in orthopaedic. Mater Des 2020;191:108608. https://doi.org/10.1016/j.matdes.2020.108608.

[6] Gómez S, Vlad MD, López J, Fernández E. Design and properties of 3D scaffolds for bone tissue engineering. Acta Biomater 2016;42:341–50. https://doi.org/10.1016/j.actbio.2016.06.032.

[7] Smolin I, Makarov P, Eremin M, Matyko K. Numerical simulation of mesomechanical behavior of porous brittle materials. Procedia Struct Integr 2016;2:3353–60. https://doi.org/10.1016/j.prostr.2016.06.418.

[8] Bruno G, Efremov AM, Levandovskyi AN, Clausen B. Connecting the macro- and microstrain responses in technical porous ceramics: modeling and experimental validations. J Mater Sci 2011;46:161–73. https://doi.org/10.1007/s10853-010-4899-0.

[9] Roberts A, Garboczi E. Elastic properties of model porous ceramics. J Am Ceram Soc 2000;83(12):3041–8. https://doi.org/10.1111/j.1151-2916.2000.tb01680.x.

[10] Torquato S. Random Heterogeneous media: microstructure and improved bounds on elastic properties. Appl Mech Rev 1991;44(2):37–76. https://doi.org/10.1115/1.3119494

[11] Konovalenko IS, Smolin AY, Korostelev SY, Psakh'e SG. Dependence of the macroscopic elastic properties of porous media on the parameters of a stochastic spatial pore distribution. Tech Phys 2009;54:758–61. https://doi.org/10.1134/S1063784209050272.

[12] Smolin I., Eremin M., Makarov P.V., Evtushenko E., Kulkov S., Buyakova S. Brittle porous material mesovolume structure models and simulation of their mechanical properties. AIP conference proceedings, vol. 1623; 2014. p. 595–598. https://doi.org/10.1063/1.4899015

[13] Du H, Yousefian O, Horn T, Muller M. Evaluation of structural anisotropy in a porous titanium medium mimicking trabecular bone structure using mode-converted ultrasonic scattering. EEE Trans Ultrason Ferroelectr Freq Control 2020;67:1017–24. https://doi.org/10.1109/TUFFC.2019.2963162.

[14] Barbas A, Bonnet AS, Lipinski P, Pesci R, Dubois G. Development and mechanical characterization of porous titanium bone substitutes. J Mech Behav Biomed Mater 2012;9:34–44. https://doi.org/10.1016/j.jmbbm.2012.01.008.

[15] Makarov PV. Evolutionary nature of destruction of solids and media. Phys Mesomech 2007;10(3–4):134–47. https://doi.org/10.1016/j.physme.2007.08.003.

[16] Makarov PV. Mathematical theory of evolution of loaded solids and media. Phys Mesomech 2008;11(5–6):213–27. https://doi.org/10.1016/j.physme.2008.11.002.

[17] Kostandov YA, Makarov PV, Eremin MO, Smolin IY, Shipovskii IE. Fracture of compressed brittle bodies with a crack. Int Appl Mech 2013;49:95–101. https://doi.org/10.1007/s10778-013-0555-0.